Abstracta

Ano XXVI - N. 02

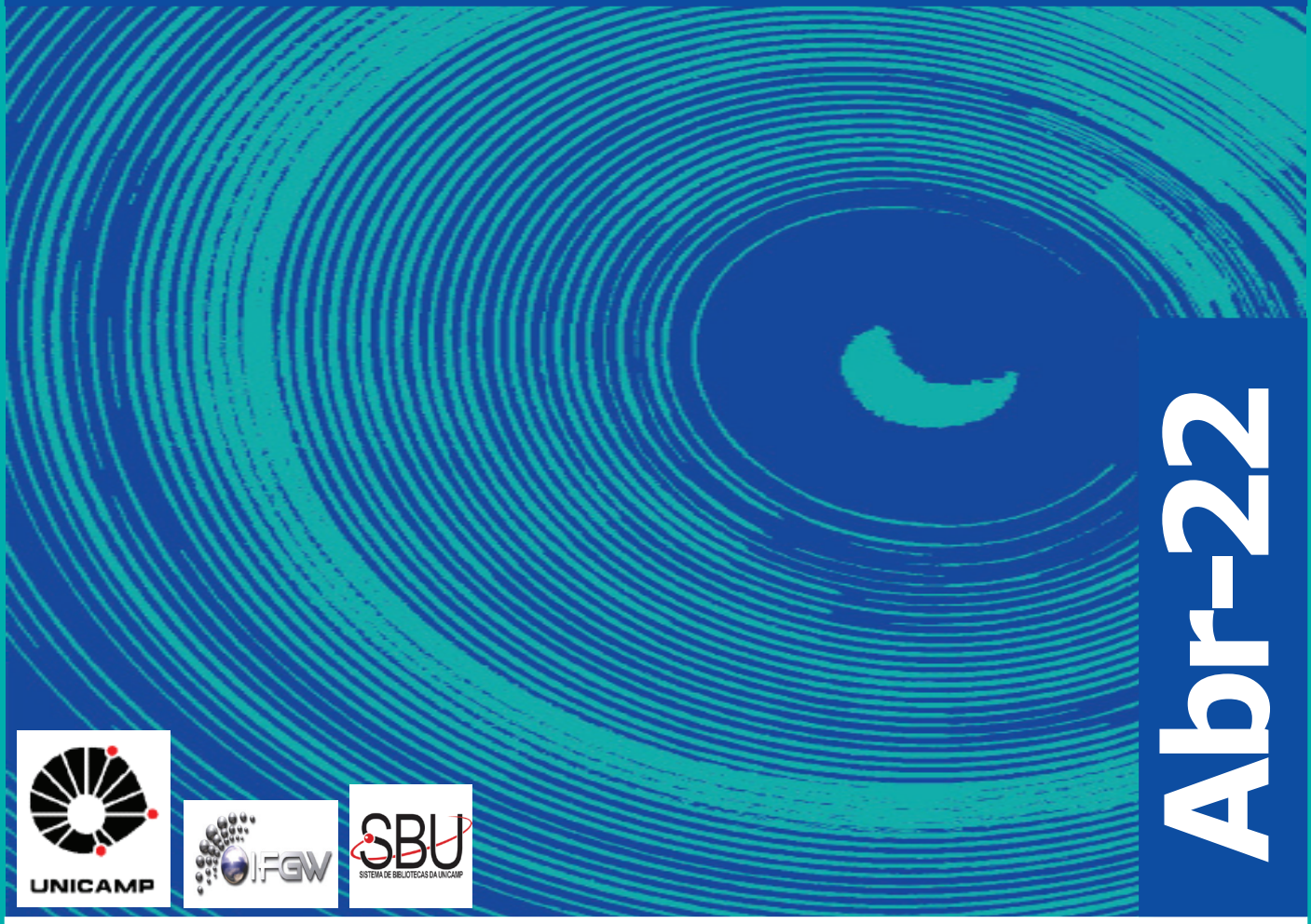

Abr-22

Artigos publicados - P034-2022 à P076-2022

Correções - C001-2022 à C002-2022

Defesas de Dissertações do IFGW - D003-2022 à D005-2022

Defesas de Teses do IFGW - T004-2022 à T008-2022

Artigos publicados

[P034-2022] "Arrhenius activation energy and transitivity in fission-track annealing equations"

Rufino, M.*; Guedes, S.*

Fission-track annealing models aim to extrapolate laboratory annealing kinetics to the geological timescale for application to geological studies. Model trends empirically capture the mechanisms of track length reduction. To facilitate the interpretation of the fission-track annealing trends, a formalism, based on quantities already in use for the study of physicochemical processes, is developed and allows for the calculation of rate constants, Arrhenius activation energies, and transitivity functions for the fission-track annealing models. These quantities are then obtained for the parallel Arrhenius, parallel curvilinear, fanning Arrhenius, and fanning curvilinear models, and fitted with Durango apatite data. Parallel models showed to be consistent with a single activation energy mechanism and a reaction-order model of order approximate to - 4. However, the fanning curvilinear model is the one that results in better fits laboratory data and predictions in better agreement with geological evidence. Fanning models seem to describe a more complex picture, with concurrent recombination mechanisms presenting activation energies varying with time and temperature, and the reaction-order model seems not to be the most appropriate. It is apparent from the transitivity analysis that the dominant mechanisms described by the fanning models are classical (not quantum) energy barrier transitions.

CHEMICAL GEOLOGY 595, 120779, 2022. DOI: 10.1016/j.chemgeo.2022.120779

[P035-2022] "Boosting engine performance with Bose-Einstein condensation"

Myers, N. M.*; Pena, F. J.; Negrete, O.; Vargas, P.; Chiara, G. de; **Deffner, S.***

At low-temperatures a gas of bosons will undergo a phase transition into a quantum state of matter known as a Bose--Einstein condensate (BEC), in which a large fraction of the particles will occupy the ground state simultaneously. Here we explore the performance of an endoreversible Otto cycle operating with a harmonically confined Bose gas as the working medium. We analyze the engine operation in three regimes, with the working medium in the BEC phase, in the gas phase, and driven across the BEC transition during each cycle. We find that the unique properties of the BEC phase allow for enhanced engine performance, including increased power output and higher efficiency at maximum power.

NEW JOURNAL OF PHYSICS 24[2], 025001, 2022. DOI: 10.1088/1367-2630/ac47cc

[P036-2022] "Chemisorption Competition between H2O and H-2 for Sites on the Si Surface under Xe+ Ion Bombardment: An XPS Study"

Antunes, V. G.*; Figueroa, C. A.; **Alvarez, F.***

This paper reports the competition of H2O (residual) and H-2 by site (defects) on the Si surface, created by Xe+ ion bombardment. X-ray photoelectron spectroscopy (XPS) in an ultrahigh vacuum system attached to the sample preparation chamber provided the data for the analyses. As hydrogen cannot be detected by XPS, an indirect method to evaluate the O and H cover ratio was developed. The hydrogen passivation effect obtained by the formation of the Si-H bond due to H-2 chemisorption limits Si-OH and Si-O-Si bonds, which are products of H2O dissociation. In addition, the results have shown that Xe+ ion bombardment diminished the H-2 chemisorption energy barrier onto Si.

LANGMUIR 38[6], 2109-2116, 2022. DOI: 10.1021/acs.langmuir.1c03189

[P037-2022] "Correlation redistribution by causal horizons"

Gioia, L. P. de*; Oliveira, M. C. de*

The Minkowski vacuum 10 > M, which for an inertial observer is devoid of particles, is perceived as a thermal bath by Rindler observers living in a single Rindler wedge (Unruh in Phys Rev D 14:870, 1976) as a result of the discrepancy in the definition of positive frequency between the two classes of observers and a strong entanglement between degrees of freedom in the left and right Rindler wedges. We revisit the problem of quantification of the correlations in a two-mode state of a free neutral scalar field which is observed by an inertial observer Alice and left/right Rindler observers Rob/AntiRob, a problem that pertains to the field of relativistic quantum information and has been previously studied in Martin-Martinez et al. (Phys Rev D 82:064006, 2010) and Datta (Phys Rev A 80:052304, 2009). We focus on the analysis of informational quantities like the locally accessible and locally inaccessible information (Koashi and Winter in Phys Rev A 69:022309, 2004; Fanchini et al. in Phys Rev A 84:012313, 2011; Fanchini et al. in New J Phys 14:013027, 2012) and a closely associated entanglement measure, the entanglement of formation. We conclude that, with respect to the correlation structure probed by inertial observers alone, the introduction of a Rindler observer gives rise to a correlation redistribution which can be quantified by the entanglement of formation. Given the informational meaning of the derived correlations, we discuss on the capacity of a quantum channel to communicate classical information between accelerated parties.

EUROPEAN PHYSICAL JOURNAL C 82[2], 152, 2022. DOI: 10.1140/epjc/s10052-022-10090-w

[P038-2022] "Dark Energy Survey Year 3 results: A 2.7% measurement of baryon acoustic oscillation distance scale at redshift 0.835"

Abbott, T. M. C.; Aguena, M.; **Brandao-Souza, A.***; et al. DES Collaboration

We present angular diameter measurements obtained by measuring the position of baryon acoustic oscillations (BAO) in an optimized sample of galaxies from the first three years of Dark Energy Survey data (DES Y3). The sample consists of 7 million galaxies distributed over a footprint of 4100 deg(2) with 0.6 < z(photo) < 1.1 and a typical redshift uncertainty of 0.03(1 +z). The sample selection is the same as in the BAO measurement with the first year of DES data, but the analysis presented here uses three times the area, extends to higher redshift, and makes a number of improvements, including a fully analytical BAO template, the use of covariances from both theory and simulations, and an extensive preunblinding protocol. We used two different statistics; angular correlation function and power spectrum, and validate our pipeline with an ensemble of over 1500 realistic simulations. Both statistics yield compatible results. We combine the likelihoods derived from angular correlations and spherical harmonics to constrain the ratio of comoving angular diameter distance D-M at the effective redshift of our sample to the sound horizon scale at the drag epoch. We obtain D-M (z(eff)= 0.835)/r(d) = 18.92 +/- 0.51, which is consistent with, but smaller than, the Planck prediction assuming flat Lambda CDM, at the level of 2.3 sigma. The analysis was performed blind and is robust to changes in a number of analysis choices.

It represents the most precise BAO distance measurement from imaging data to date, and is competitive with the latest transverse ones from spectroscopic samples at z > 0.75. When combined with DES 3x2pt + SNIa, they lead to improvements in H-0 and Omega(m) constraints by similar to 20%.

PHYSICAL REVIEW D 105[4], 043512, 2022. DOI: 10.1103/PhysRevD.105.043512

[P039-2022] "Dark Energy Survey Year 3 results: Cosmological constraints from galaxy clustering and weak lensing"

Abbott, T. M. C.; Aguena, M.; **Brandao-Souza, A.*; Navarro--Alsina, A.***; et al. DES Collaboration

We present the first cosmology results from large-scale structure using the full 5000 deg(2) of imaging data from the Dark Energy Survey (DES) Data Release 1. We perform an analysis of large-scale structure combining three two-point correlation functions (3 x 2pt): (i) cosmic shear using 100 million source galaxies, (ii) galaxy clustering, and (iii) the cross-correlation of source galaxy shear with lens galaxy positions, galaxy--galaxy lensing. To achieve the cosmological precision enabled by these measurements has required updates to nearly every part of the analysis from DES Year 1, including the use of two independent galaxy clustering samples, modeling advances, and several novel improvements in the calibration of gravitational shear and photometric redshift inference. The analysis was performed under strict conditions to mitigate confirmation or observer bias; we describe specific changes made to the lens galaxy sample following unblinding of the results and tests of the robustness of our results to this decision. We model the data within the flat Lambda CDM and wCDM cosmological models, marginalizing over 25 nuisance parameters. We find consistent cosmological results between the three two-point correlation functions; their combination yields clustering amplitude S-8 = 0.776(-0.017)(+0.017) and matter density Omega(m) = 0.339(-0.031)(+0.032) in Lambda CDM, mean with 68% confidence limits; S-8 = 0.775(-0.024)(+0.026), Omega(m) = 0.352(-0.041)(+0.035), and dark energy equation-of-state parameter w = -0.98(-0.02)(+0.32) in wCDM. These constraints correspond to an improvement in signal-to--noise of the DES Year 33 x 2pt data relative to DES Year 1 by a factor of 2.1, about 20% more than expected from the increase in observing area alone. This combination of DES data is consistent with the prediction of the model favored by the Planck 2018 cosmic microwave background (CMB) primary anisotropy data, which is quantified with a probability-to-exceed p = 0.13-0.48. We find better agreement between DES 3 x 2pt and Planck than in DES Y1, despite the significantly improved precision of both. When combining DES 3 x 2pt data with available baryon acoustic oscillation, redshift-space distortion, and type la supernovae data, we find p = 0.34. Combining all of these datasets with Planck CMB lensing yields joint parameter constraints of S-8 = 0.812(-0.008)(+0.008), Omega(m) = 0.306(-0.005)(+0.004), h = 0.680(-0.003)(+0.004), and Sigma m(nu) < 0.13 eV (95% C.L.) in Lambda CDM; S-8 = 0.812(-0.008)(+0.008), Omega(m) = 0.302(-0.006)(+0.006), h = 0.687(-0.007)(+0.006), and w = -1.031(-0.027)(+0.030) in wCDM.

PHYSICAL REVIEW D 105[2], 023520, 2022. DOI: 10.1103/PhysRevD.105.023520

[P040-2022] "Dark Energy Survey Year 3 results: Cosmology from cosmic shear and robustness to data calibration"

Amon, A.; Gruen, D.; **Navarro-Alsina, A.***; et al. DES Collaboration

This work, together with its companion paper, Secco, Samuroff et al. [Phys. Rev. D 105, 023515 (2022)], present the Dark Energy Survey Year 3 cosmic-shear measurements and cosmological constraints based on an analysis of over 100 million source galaxies. With the data spanning 4143 deg(2) on the sky, divided into four redshift bins, we produce a measurement with a signal-to-noise of 40. We conduct a blind analysis in the context of the Lambda-Cold Dark Matter (Lambda CDM) model and find a 3% constraint of the clustering amplitude, S-8 sigma(8)(Omega(m)/0.3)(0.5) = 0.759(-0.023)(+0.025). A Lambda CDM-Optimized analysis, which safely includes smaller scale information, yields a 2% precision measurement of S-8 = 0.772(-0.017)(+0.018) that is consistent with the fiducial case. The two low-redshift measurements are statistically consistent with the Planck Cosmic Microwave Background result, however, both recovered S-8 values are lower than the high-redshift prediction by 2.3 sigma and 2.1 sigma (p-values of 0.02 and 0.05), respectively. The measurements are shown to be internally consistent across redshift bins, angular scales and correlation functions. The analysis is demonstrated to be robust to calibration systematics, with the S-8 posterior consistent when varying the choice of redshift calibration sample, the modeling of redshift uncertainty and methodology. Similarly, we find that the corrections included to account for the blending of galaxies shifts our best-fit S-8 by 0.5 sigma without incurring a substantial increase in uncertainty. We examine the limiting factors for the precision of the cosmological constraints and find observational systematics to be subdominant to the modeling of astrophysics. Specifically, we identify the uncertainties in modeling baryonic effects and intrinsic alignments as the limiting systematics.

PHYSICAL REVIEW D 105[2], 023514, 2022. DOI: 10.1103/PhysRevD.105.023514

[P041-2022] "Dark Energy Survey Year 3 results: Cosmology from cosmic shear and robustness to modeling uncertainty"

Secco, L. F.; Samuroff, S.; **Brandao-Souza, A.*; Alsina, A. Navarro***; et al. DES Collaboration

This work and its companion paper, Amon et al. [Phys. Rev. D 105, 023514 (2022)], present cosmic shear measurements and cosmological constraints from over 100 million source galaxies in the Darki Energy Survey (DES) Year 3 data. We constrain the lensing amplitude parameter S-8 equivalent to sigma(8)root Omega(m)/0.3 at the 3% level in Lambda CDM: S-8 = 0.759(-0.023)(+0.025) (68% CL). Our constraint is at the 2% level when using angular scale cuts that are optimized for the Lambda CDM analysis: S-8 = 0.772(-0.017)(+0.018) (68% CL). With cosmic shear alone, we find no statistically significant constraint on the dark energy equation-of-state parameter at our present statistical power. We carry out our analysis blind, and compare our measurement with constraints from two other contemporary weak lensing experiments: the Kilo-Degree Survey (KiDS) and Hyper-Suprime Camera Subaru Strategic Program (HSC). We additionally quantify the agreement between our data and external constraints from the Cosmic Microwave Background (CMB). Our DES Y3 result under the assumption of ACDM is found to be in statistical agreement with Planck 2018, although favors a lower S-8 than the CMB-inferred value by 2.3 sigma (a p -value of 0.02). This paper explores the robustness of these cosmic shear results to modeling of intrinsic alignments, the matter power spectrum and baryonic physics. We additionally explore the statistical preference of our data for intrinsic alignment models of different complexity. The fiducial cosmic shear model is tested using synthetic data, and we report no biases greater than 0.3 sigma in the plane of S-8 x Omega(m) caused by uncertainties in the theoretical models.

PHYSICAL REVIEW D 105[2], 023515, 2022. DOI: 10.1103/PhysRevD.105.023515

[P042-2022] "Dark energy survey year 3 results: Cosmology with peaks using an emulator approach"

Zuercher, D.; Fluri, J.; **Navarro-Alsina, A.***; et al. DES Collaboration

We constrain the matter density Omega(m) and the amplitude of density fluctuations sigma(s) within the Lambda CDM cosmological model with shear peak statistics and angular convergence power spectra using mass maps constructed from the first three years of data of the Dark Energy Survey (DES Y3). We use tomographic shear peak statistics, including cross-peaks: peak counts calculated on maps created by taking a harmonic space product of the convergence of two tomographic redshift bins. Our analysis follows a forward-modelling scheme to create a likelihood of these statistics using N-body simulations, using a Gaussian process emulator. We take into account the uncertainty from the remaining, largely unconstrained Lambda CDM parameters (Omega(b), n(s), and h). We include the following lensing systematics: multiplicative shear bias, photometric redshift uncertainty, and galaxy intrinsic alignment. Stringent scale cuts are applied to avoid biases from unmodelled baryonic physics. We find that the additional non-Gaussian information leads to a tightening of the constraints on the structure growth parameter yielding S-8 sigma(8)root Omega(m)/0.3 = 0.797(-0.013)(+0.015) (68 per cent confidence limits), with a precision of 1.8 per cent, an improvement of 38 per cent compared to the angular power spectra only case. The results obtained with the angular power spectra and peak counts are found to be in agreement with each other and no significant difference in S-8 is recorded. We find a mild tension of 1.5 a between our study and the results from Planck 2018, with our analysis yielding a lower S-8. Furthermore, we observe that the combination of angular power spectra and tomographic peak counts breaks the degeneracy between galaxy intrinsic alignment A(IA) and S-8, improving cosmological constraints. We run a suite of tests concluding that our results are robust and consistent with the results from other studies using DES Y3 data.

MONTHLY NOTICES OF THE ROYAL ASTRONOMICAL SOCIETY 511[2], 2075-2104, 2022. DOI: 10.1093/mnras/stac078

[P043-2022] "Design, construction and operation of the ProtoDUNE-SP Liquid Argon TPC"

Abud, A. A.; Abi, B.; **Belchior, E.*; Holanda, P. C. de*; Souza, G. de*; Garcia, A. C. B.*; Gelli, B.*; Giammaria, P.*; Guzzo, M. M.*; Kemp, E.*; Machado, A. A.*; Peres, O. L. G.*; Prakash, S.*; Bazetto, M. C. Q.*; Segreto, E.*; Souza, H. V. de***; et al. DUNE Collaboration

The ProtoDUNE-SP detector is a single-phase liquid argon time projection chamber (LArTPC) that was constructed and operated in the CERN North Area at the end of the H4 beamline. This detector is a prototype for the first far detector module of the Deep Underground Neutrino Experiment (DUNE), which will be constructed at the Sandford Underground Research Facility (SURF) in Lead, South Dakota, U.S.A. The ProtoDUNE-SP detector incorporates full-size components as designed for DUNE and has an active volume of 7 x 6 x 7.2 m3. The H4 beam delivers incident particles with well-measured momenta and high-purity particle identification. ProtoDUNE-SP's successful operation between 2018 and 2020 demonstrates the effectiveness of the single-phase far detector design. This paper describes the design, construction, assembly and operation of the detector components.

JOURNAL OF INSTRUMENTATION 17[1], P01005, 2022. DOI: 10.1088/1748-0221/17/01/P01005

[P044-2022] "Different desorption rates prompting an indirect isotopic effect on nanoscale friction"

Leidens, L. M.; Matte, D.; Rech, G. L.; Zorzi, J. E.; Michels, A. F.; **Alvarez, F.***; Perottoni, C. A.; Figueroa, C. A.

Friction behavior at the nanoscale may be split into different contributions, including phononic dissipation. Despite the isotopic effect in the phononic component being previously explored, experimental and theoretical approaches determined contradictory conclusions. Here, a desorption-based model is proposed, and it is found to be consistent with previously published experimental data on hydrogenated and/or deuterated amorphous carbon films. Moreover, molecular dynamics simulations showed that a surface coverage difference as low as 5% might promote an effect on friction even greater than that observed experimentally. This happens when reactive defects are created after desorption (prompting carbon dangling bonds), reinforcing the assumption that minor surface differences may be sufficient for the effects observed, meeting both experimental and theoretical approaches in the same overall trend. Therefore, the phononic dissipation occurs, but the isotopic effect may be indirect, where the desorption rate of hydrogen and deuterium plays a role by exposing carbon dangling bonds, changing the interface of interaction and the nanoscale friction ultimately.

APPLIED SURFACE SCIENCE ADVANCES 7[SI], 100201, 2022. DOI: 10.1016/j.apsadv.2021.100201

[P045-2022] "Dissociative electron attachment to 5-bromo--uracil: non-adiabatic dynamics on complex-valued potential energy surfaces"

Cornetta, L. M.*; Martinez, T. J.; Varella, M. T. D.

Electron induced dissociation reactions are relevant to many fields, ranging from prebiotic chemistry to cancer treatments. However, the simulation of dissociation electron attachment (DEA) dynamics is very challenging because the auto-ionization widths of the transient negative ions must be accounted for. We propose an adaptation of the ab initio multiple spawning (AIMS) method for complex-valued potential energy surfaces, along the lines of recent developments based on surface hopping dynamics. Our approach combines models for the energy dependence of the auto-ionization widths, obtained from scattering calculations, with survival probabilities computed for the trajectory basis functions employed in the AIMS dynamics. The method is applied to simulate the DEA dynamics of 5-bromouracil in full dimensionality, i.e., taking all the vibrational modes into consideration. The propagation starts on the pi(2)* resonance state and describes the formation of Br- anions mediated by non-adiabatic couplings. The potential energies, gradients and non-adiabatic couplings were computed with the fractional-occupancy molecular orbital complete-active-space configuration-interaction method, and the calculated DEA cross section are consistent with the observed DEA intensities.

PHYSICAL CHEMISTRY CHEMICAL PHYSICS 24[11], 6845-6855, 2022. DOI: 10.1039/d1cp05663h

[P046-2022] "Dynamics and structural transformations of carbon onion-like structures under high-velocity impacts"

Pereira Junior, M. L.; Cunha, W. F. da; Sousa Junior, R. T. de; Nze, G. D. A.; **Galvao, D. S.***; Ribeiro, J. L.

Carbon nano-onions (CNO) are multilayered fullerenes. They exhibit good electrical conductivity and large surface area, being of interest for several optoelectronic applications. However, it is still an open question what synthesis routes can be used to convert them into diamonds. Here, we used fully atomistic reactive (ReaxFF) molecular dynamics simulations to study the dynamics and structural transformations of CNO structures under high-velocity impacts against a fixed and rigid substrate.

The aim of this study is to propose a new synthesis route, based on the mechanical impact of CNO, that can be exploited in the conversion of onions to diamonds. Our results indicated three regimes formed after the CNO impact: slightly deformed CNO (quasi-elastic collision, below 2.0 km/s), collapsed CNO (inelastic collisions, between 3.0 and 5.0 km/s) forming a diamondoid-like core, and fragmented CNO yielding linear atomic carbon chains (above 5.0 km/s). We also discussed the dynamical reconfiguration of carbon-carbon bonds during the collision process. The impact of CNO yielded sp(3)-like bond types for all the used initial velocities. At intermediate velocities (between 3.0 and 5.0 km/s), the inelastic collision forms diamondoid-like cores by converting a substantial quantity of sp(2)-like bonds into sp(3)-like ones.

CARBON 189, 422-429, 2022. DOI: 10.1016/j.carbon.2021.12.064

[P047-2022] "Entanglement-based quantum communication complexity beyond Bell nonlocality"

Ho, J.; Moreno, G.; Brito, S.; Graffitti, F.; Morrison, C. L.; Nery, R.; Pickston, A.; Proietti, M.; **Rabelo, R.***; Fedrizzi, A.; Chaves, R.

Efficient distributed computing offers a scalable strategy for solving resource-demanding tasks, such as parallel computation and circuit optimisation. Crucially, the communication overhead introduced by the allotment process should be minimised-a key motivation behind the communication complexity problem (CCP). Quantum resources are well-suited to this task, offering clear strategies that can outperform classical counterparts. Furthermore, the connection between quantum CCPs and non-locality provides an information--theoretic insight into fundamental quantum mechanics. Here we connect quantum CCPs with a generalised non-locality framework-beyond Bell's paradigmatic theorem-by incorporating the underlying causal structure, which governs the distributed task, into a so-called non-local hidden-variable model. We prove that a new class of communication complexity tasks can be associated with Bell-like inequalities, whose violation is both necessary and sufficient for a quantum gain. We experimentally implement a multipartite CCP akin to the guess-your-neighbour-input scenario, and demonstrate a quantum advantage when multipartite Greenberger--Horne-Zeilinger (GHZ) states are shared among three users.

NPJ QUANTUM INFORMATION 8[1], 13, 2022. DOI: 10.1038/s41534-022-00520-8

[P048-2022] "Evidence for X(3872) in Pb-Pb Collisions and Studies of its Prompt Production at root s(NN)=5.02 TeV"

Sirunyan, A. M.; Tumasyan, A.; **Chinellato, J. A.*; Tonelli Manganote, E. J.***; et al.; CMS Collaboration

The first evidence for X(3872) production in relativistic heavy ion collisions is reported. The X(3872) production is studied in lead-lead (Pb-Pb) collisions at a center-of-mass energy of root s(NN) = 5.02 TeV per nucleon pair, using the decay chain X(3872) -> J/psi pi(+)pi(-) -> mu(+) mu(-) pi(+)pi(-). The data were recorded with the CMS detector in 2018 and correspond to an integrated luminosity of 1.7 nb(-1). The measurement is performed in the rapidity and transverse momentum ranges vertical bar y vertical bar < 1.6 and 15 < p(T) < 50 GeV/c. The significance of the inclusive X(3872) signal is 4.2 standard deviations. The prompt X(3872) to psi 2S yield ratio is found to be rho(Pb-Pb) = 1.08 +/- 0.49(stat) +/- 0.52(syst), to be compared with typical values of 0.1 for pp collisions. This result provides a unique experimental input to theoretical models of the X(3872) production mechanism, and of the nature of this exotic state.

PHYSICAL REVIEW LETTERS 128[3], 032001, 2022. DOI: 10.1103/PhysRevLett.128.032001

[P049-2022] "Evidencing the formation of Pt nano-islands on Cr2O3/Ag(111)"

Kilian, A. S.; Abreu, G. J.; **Siervo, A. de*; Landers, R.***; Morais, J.

The present work reports on a comprehensive surface atomic structure investigation on a Pt/Cr2O3/Ag(111) model catalyst. Molecular beam epitaxy (MBE) was applied to achieve the Pt/Cr2O3 model system, and in situ characterization via X-ray photoelectron spectroscopy (XPS), low-energy electron diffraction (LEED) and X-ray photoelectron diffraction (XPD) allowed for probing its outermost layers' properties. XPD provided valuable element-specific short-range information from the Pt/Cr2O3/Ag(111) surface, and the results were compared to a precise and systematic multiple scattering simulation approach. The experiments, characterizations and simulations suggest strong evidence of Pt nanoisland formation on the Cr2O3/Ag(111) surface. The results indicated that these nanoislands typically consist of three Pt monolayer thick clusters with considerable structural variations in their interatomic layer distances. Such an atomic rearrangement could clarify the high reactivity observed in heterogeneous catalysts containing Pt nanoparticles coalesced or dispersed on oxide substrates.

CRYSTENGCOMM 24[12], 2270-2279, 2022. DOI: 10.1039/d1ce01628h

[P050-2022] "Gradual and selective achievement of Rutile--TiO2 by thermal annealing amorphous TixOyNz films"

Zanatta, A. R.; **Echeverrigaray, F. G.*; Cemin, F.*; Alvarez, F.***

To a large extent, future technological progress relies on the study-development of advanced materials with new and/or improved properties. The semiconductors titanium oxynitride (TixOyNz) and titanium dioxide (TiO2) perfectly meet these requirements in the sense that their main chemical and structural properties can be customized, leading to successful contributions in optics, electronics, catalysis, bactericides surfaces, and photovoltaics applications, for instance. Motivated by these aspects, this paper reports on the structure and optical bandgap of TixOyNz, as obtained by Raman scattering and optical transmittance spectroscopy, respectively. The study comprises a set of films produced by N-2-plasma Ti sputtering and subsequently thermal annealed in an atmosphere of oxygen flux. As the thermal treatments advance, the Raman spectra indicate a gradual transformation of the films from amorphous+(nano/micro-)crystalline TixOyNz to the crystalline Rutile phase of TiO2 (R-TiO2). Consistent with these structural changes, the optical bandgap of the films decreases from - 3.2 to 2.5 eV, i.e., across part of the ultraviolet-blue spectral region. The analysis of the experimental data confirms the importance of nitrogen (in the early stages of sample preparation) on the achievement of R-TiO2 in a continuous and controllable way. Therefore, this paper shows the suitability of the TixOyNz compound to produce films with well-defined crystalline TiO2-related structures and specific optical bandgap values.

JOURNAL OF NON-CRYSTALLINE SOLIDS 579, 121375, 2022. DOI: 10.1016/j.jnoncrysol.2021.121375

[P051-2022] "High-temperature oxidation behaviour of nanostructure surface layered austenitic stainless steel"

Singh, D.; **Cemin, F.*; Jimenez, M. J. M.*; Antunes, V.*; Alvarez, F.*;** Orlov, D.; Figueroa, C. A.; Hosmani, S. S.

The present study investigates the high-temperature oxidation behaviour of nanostructure surface layered AISI 304L stainless steel. A severely deformed layer of -300 mu m thickness, consisting of nanoscale grains (-40 nm size) in the topmost region, is successfully developed using the surface mechanical attrition treatment (SMAT) process. The SMATed layer is substantially stable up to 700 degrees C; however, the surface hardness is reduced by -37% at 800 degrees C for 25 h oxidation duration. Glow discharge optical emission spectroscopy and X-ray photoelectron spectroscopy analysis revealed the considerable difference in the chemistry and elemental distribution across the oxide scale of SMATed and non-SMATed specimens. Adherent, denser, and thinner scale, dominated by nanocrystals of Cr- and Mn-rich oxides, is formed on the SMATed steel. However, the Fe--oxide dominated scale containing micro-crystals is found on the non-SMATed specimens, which shows noticeable exfoliation. A high density of grain boundaries and lattice defects in the SMATed layer display admirable reactive diffusion properties of Cr and Mn during oxidation of steel, instigating the formation of a protective oxide scale. The SMATed specimens exhibit multiple zones in the oxide scale: (i) Cr/Mn depleted outer layer, (ii) Cr-/Mn-rich inner layer, and (iii) gradually decreasing Cr/Mn region.

APPLIED SURFACE SCIENCE 581, 152437, 2022. DOI: 10.1016/j.apsusc.2022.152437

[P052-2022] "Inclusive and differential cross section measurements of single top quark production in association with a Z boson in proton-proton collisions at root s=13 TeV"

Tumasyan, A.; Adam, W.; **Chinellato, J. A.***; et al. CMS Collaboration

Inclusive and differential cross sections of single top quark production in association with a Z boson are measured in proton-proton collisions at a center-of-mass energy of 13 TeV with a data sample corresponding to an integrated luminosity of 138 fb(-1) recorded by the CMS experiment. Events are selected based on the presence of three leptons, electrons or muons, associated with leptonic Z boson and top quark decays. The measurement yields an inclusive cross section of 87.9(-7.3)(+7.5) (stat)(-6.0)(+7.3)(syst) fb for a dilepton invariant mass greater than 30 GeV, in agreement with standard model (SM) calculations and represents the most precise determination to date. The ratio between the cross sections for the top quark and the top antiquark production in association with a Z boson is measured as 2.37(-0.42)(+0.56)(stat)(-0.13)(+0.27) (syst). Differential measurements at parton and particle levels are performed for the first time. Several kinematic observables are considered to study the modeling of the process. Results are compared to theoretical predictions with different assumptions on the source of the initial-state b quark and found to be in agreement, within the uncertainties. Additionally, the spin asymmetry, which is sensitive to the top quark polarization, is determined from the differential distribution of the polarization angle at parton level to be 0.54 +/- 0.16 (stat)+/- 0.06 (syst), in agreement with SM predictions.

JOURNAL OF HIGH ENERGY PHYSICS [2], 107, 2022. DOI: 10.1007/JHEP02(2022)107

[P053-2022] "Influence of Anomalous Changes in the Crystal Structure on the Transport Properties of YbNi1-xCuxAl Series of Alloys"

Pupo, D. R.; **Gandra, F. G.*;** Barquin, L. F.

Results of the transport properties of the YbNi1-xCuxAl (x = 0, 0.2, 0.5, 0.8 and 1.0) series of alloys are reported. The previous analysis of X-ray diffraction patterns indicates that all compounds crystallize in the hexagonal ZrNiAl structure with a linear behavior of the unit cell volume as a function of the Cu concentration (x). This is not found in the unit cell parameters, showing a discontinuity between x = 0.5 and 0.8. Such discontinuities affect the behavior of the electrical resistivity, in which the position of the minimum temperature changes from 95 K to 175 K, and a rise in the low temperature slope in the magnetic contribution (with -lnT dependence) from 21 mu omega cm to 212 mu omega cm is observed. In addition, the electronic coefficient of the specific heat increases almost twofold from 125 mJ/mol center dot K-2 (x = 0.5) to 246 mJ/mol center dot K-2 (x = 0.8). These changes are attributed to the variation of the distance between Yb and transition metals (Ni and Cu) along the series and the different electronic properties of the transition metals (Ni and Cu).

MATERIALS 15[5], 1688, 2022. DOI: 10.3390/ma15051688

[P054-2022] "Investigation of Chloroquine Resinate Feasibility and In Vitro Taste Masking Evaluation for Pediatric Formulations"

Guimaraes, T. F.; Vital, I. C. F.; Sousa, E. G. R. de; Boniatti, J.; Bandini, T. B.; Carr, O.; Oliveira Jr, O. N.; **Shimizu, F. M.***; Fonseca, L. B. da; Vicosa, A. L.

In this study, chloroquine resinates were prepared at a 1:1 (w:w) drug-to-resin ratio using the batch method with polacrilex (PC), sodium polystyrene sulfonate (SPS), and polacrilin potassium (PP) ion exchange resins (IER). The influence of drug/resin ratio and pH of the medium on drug loading efficiency was explored. UV-VIS spectrophotometric analysis showed that SPS resin had high loading efficiency for chloroquine diphosphate (CLP), above 89%, regardless of the pH. PP resin was more effective at pH 5.0 (90.68%) than at pH 1.0 (2.09%), and PC resin had only 27.63% of CLP loading efficiency. CLP complexation with IER yielded amorphous mixtures according to results from differential scanning calorimetry (DSC) and X--ray powder diffraction (XRPD), thus indicating drug-resin interaction. The taste masking efficiency was evaluated with in vitro methods using an adapted dissolution test and an electronic tongue system. During dissolution tests, SPS released only 1.0% of CLP after 300 s, while PP released over 10% after 90 s in simulated saliva solution. The electronic tongue distinguished the samples containing CLP, resins, and resinates by using multidimensional projection techniques that indicated an effective drug taste masking. In an accelerated stability study, the drug contents did not decrease in chloroquine resinates, and there was no physical degradation of the resinates after 60 days. Using chloroquine resinates therefore represents a novel way to evaluate taste masking in vitro which is relevant for the early formulation development process.

AAPS PHARMSCITECH 23[2], 69, 2022. DOI: 10.1208/s12249-022-02219-7

[P055-2022] "Is It Possible to Follow the Structural Evolution of Water in "No-Man's Land" Using a Pulsed-Heating Procedure?"

Ribeiro, I. de A.*; Koning, M. de*; Molinero, V.

The anomalous increase in compressibility and heat capacity of supercooled water has been attributed to its structural transformation of into a four-coordinated liquid. Experiments revealed that kappa(T) and C-p peak at T-W(thermo) approximate to 229 K [Kim et al. Science 2017, 358, 1589; Pathak et al. Proc. Natl. Acad. Sci. 2021, 118, e2018379118]. Recently, a pulsed heating procedure (PHP) was employed to interrogate the structure of water, reporting a steep increase in tetrahedrality around T-W(PHP) = 210 +/- 3 K [Kringle et al. Science 2020, 369, 1490]. This discrepancy questions whether water structure and thermodynamics are decoupled, or if the shift in T-W is an artifact of PHP. Here we implement PHP in molecular simulations.

We find that the stationary states captured at the bottom of the pulse are not representative of the thermalized liquid or its inherent structure. Our analysis reveals a temperature-dependent distortion that shifts T-W(PHP) to similar to 20 K below T--W(thermo). We conclude that 2 orders of magnitude faster rates are required to sample water's inherent structure with PHP.

JOURNAL OF PHYSICAL CHEMISTRY LETTERS 13[4], 1085-1089, 2022. DOI: 10.1021/acs.jpclett.1c04106

[P056-2022] "Magnetic relaxation in nanocrystalline systems: linking Monte Carlo steps with time"

Vargas, P.; **Knobel, M.***; Altbir, D.

The magnetic relaxation of a noninteracting two-dimensional ensemble of magnetic nanoparticles is simulated as a function of temperature using a Monte Carlo technique. By properly fitting the decay of magnetization using real parameters it is possible to make, at any finite temperature, a clear correspondence between Monte Carlo steps and time measured in seconds. The results allow one to visualize the intrinsic problems related to the simulation of nonequilibrium systems, and to understand the limits and range of validity of a particular system.

INTERNATIONAL JOURNAL OF MATERIALS RESEARCH 93[10], 974-977, 2022. DOI: 10.1515/ijmr-2002-0169

[P057-2022] "Measurement and QCD analysis of double-differential inclusive jet cross sections in proton-proton collisions at root s=13 TeV"

Tumasyan, A.; Adam, W.; **Chinellato, J. A.***; et al. CMS Collaboration

A measurement of the inclusive jet production in proton-proton collisions at the LHC at root s = 13TeV is presented. The double--differential cross sections are measured as a function of the jet transverse momentum p(T) and the absolute jet rapidity vertical bar y vertical bar. The anti- k(T) clustering algorithm is used with distance parameter of 0.4 (0.7) in a phase space region with jet p(T) from 97 GeV up to 3.1TeV and vertical bar y vertical bar < 2.0. Data collected with the CMS detector are used, corresponding to an integrated luminosity of 36.3 fb(-1) (33.5 fb(-1)). The measurement is used in a comprehensive QCD analysis at next-to-next-to-leading order, which results in significant improvement in the accuracy of the parton distributions in the proton. Simultaneously, the value of the strong coupling constant at the Z boson mass is extracted as alpha(S)(m(Z)) = 0.1170 +/- 0.0019. For the first time, these data are used in a standard model effective field theory analysis at next-to--leading order, where parton distributions and the QCD parameters are extracted simultaneously with imposed constraints on the Wilson coefficient c(1) of 4-quark contact interactions.

JOURNAL OF HIGH ENERGY PHYSICS [2], 142, 2022. DOI: 10.1007/JHEP02(2022)142

[P058-2022] "Measurement of the Groomed Jet Radius and Momentum Splitting Fraction in pp and Pb-Pb Collisions at root S-NN=5.02 TeV"

Acharya, S.; Adamova, D.; **Chinellato, D. D.*; Guardiano, G. G.*; Jahnke, C.*; Takahashi, J.*;** et al. Large Ion Collider Expt Collaborat

This article presents groomed jet substructure measurements in pp and Pb-Pb collisions at root s(NN)= 5.02 TeV with the ALICE detector. The soft drop grooming algorithm provides access to the hard parton splittings inside a jet by removing soft wide-angle radiation. We report the groomed jet momentum splitting fraction, z(g), and the (scaled) groomed jet radius, theta(g). Charged--particle jets are reconstructed at midrapidity using the anti--k(T) algorithm with resolution parameters R = 0.2 and R = 0.4. In heavy-ion collisions, the large underlying event poses a challenge for the reconstruction of groomed jet observables, since fluctuations in the background can cause groomed parton splittings to be misidentified. By using strong grooming conditions to reduce this background, we report these observables fully corrected for detector effects and background fluctuations for the first time. A narrowing of the theta(g) distribution in Pb-Pb collisions compared to pp collisions is seen, which provides direct evidence of the modification of the angular structure of jets in the quark-gluon plasma. No significant modification of the z(g) distribution in Pb-Pb collisions compared to pp collisions is observed. These results are compared with a variety of theoretical models of jet quenching, and provide constraints on jet energy-loss mechanisms and coherence effects in the quark-gluon plasma.

PHYSICAL REVIEW LETTERS 128[10], 102001, 2022. DOI: 10.1103/PhysRevLett.128.102001

[P059-2022] "Measurement of the Inclusive and Differential Higgs Boson Production Cross Sections in the Decay Mode to a Pair of tau Leptons in pp Collisions at root s=13 TeV"

Tumasyan, A.; Adam, W.; **Chinellato, J. A.***; et al. CMS Collaboration

Measurements of the inclusive and differential fiducial cross sections of the Higgs boson are presented, using the tau lepton decay channel. The differential cross sections are measured as functions of the Higgs boson transverse momentum, jet multiplicity, and transverse momentum of the leading jet in the event, if any. The analysis is performed using proton--proton collision data collected with the CMS detector at the LHC at a center-of-mass energy of 13 TeV and corresponding to an integrated luminosity of 138 fb-1. These are the first differential measurements of the Higgs boson cross section in the final state of two tau leptons. In final states with a large jet multiplicity or with a Lorentz-boosted Higgs boson, these measurements constitute a significant improvement over measurements performed in other final states.

PHYSICAL REVIEW LETTERS 128[8], 081805, 2022. DOI: 10.1103/PhysRevLett.128.081805

[P060-2022] "Measurement of W-+/-gamma differential cross sections in proton-proton collisions at root s=13 TeV and effective field theory constraints"

Tumasyan, A.; Adam, W.; **Chinellato, J. A.***; et al. CMS Collaboration

Differential cross section measurements of W(+/-)y production in proton-proton collisions at root s = 13 TeV are presented. The data set used in this study was collected with the CMS detector at the CERN LHC in 2016-2018 with an integrated luminosity of 138 fb(-1). Candidate events containing an electron or muon, a photon, and missing transverse momentum are selected. The measurements are compared with standard model predictions computed at next-to-leading and next-to-next-to-leading orders in perturbative quantum chromodynamics. Constraints on the presence of TeV-scale new physics affecting the WW gamma vertex are determined within an effective field theory framework, focusing on the O-3w operator. A simultaneous measurement of the photon transverse momentum and the azimuthal angle of the charged lepton in a special reference frame is performed.

This two-dimensional approach provides up to a factor of ten more sensitivity to the interference between the standard model and the O-3w contribution than using the transverse momentum alone.

PHYSICAL REVIEW D 105[5], 052003, 2022. DOI: 10.1103/PhysRevD.105.052003

[P061-2022] "Nanostructured lipid carriers for delivery of free phytosterols: Effect of lipid composition and chemical interesterification on physical stability"

Silva, M. G. da; Godoi, K. R. R. de; Gigante, M. L.; **Cardoso, L. P.*;** Ribeiro, A. P. B.

The objective of this study was to develop new nanostructured lipid carrier (NLC) formulations loaded with free phytosterols (FPs) using interesterified and simple lipid phases. The simple and interesterified lipid phases were composed of soybean oil as liquid lipid and fully hydrogenated palm (HPO) and crambe (HCO) oils s solid lipids. High-pressure homogenization was the preparation method, with soy lecithin as a natural emulsifier. The characteristics of NLCs were influenced by chemical interesterification and the composition of solid lipid, mainly with respect to the fatty acid chain size. All developed FP-loaded NLCs displayed an appropriate nanoscale size from approximately 167 to 330 nm (d(32)) and appropriate physical stability with zeta potential values ranging from -29.83 to -43.70 mV after 30 days of storage. The changes observed in these parameters were influenced by the lipid phase of the NLCs and the crystallization of FP on the surface of the NLCs. FP-loaded NLCs formulated with interesterified blends displayed smaller particle size values, with less evidence of particle agglomeration and higher absolute zeta potential values than NLCs formulated with simple blends. These results indicated that NLCs developed with interesterified lipid blends were more stable than those developed with single blends NLCs produced from solid lipids with fatty acids with larger chain sizes (HCO) had larger particle sizes but were less likely to flocculate and coalesce. Thermal behavior study revealed that interesterification caused a reduction in the melting temperature and recrystallization index of the NLCs. These findings indicated decreased crystallinity and a less organized structure. This behavior favored the highest encapsulation efficiency and load capacity observed for NLCs developed with interesterified blends.

COLLOIDS AND SURFACES A-PHYSICOCHEMICAL AND ENGINEERING ASPECTS 640, 128425, 2022. DOI: 10.1016/j.colsurfa.2022.128425

[P062-2022] "New routes in the formation of positively charged fragments upon electron attachment"

Mendes, M.; Nunes, A.; Pereira-da-Silva, J.; Rodrigues, R.; Araujo, J. M. M.; Sillva, F. Ferreira de; **Cornetta, L. M.***

Electron-driven reactions of CF3CH2F have been studied focusing on the formation of the parent cation, CF3+ and CH2F+ (C-C bond cleavage) fragments as a function of the electron energy. For the three referred cations, an unpredicted shoulder structure is observed in the ion yield between 12 and 20 eV, indicating a resonant process (electron attachment). Viewing the observations as the result of a competition between the expected dissociative electron ionization and a dissociative electron attachment, we propose a new route where the formation of the transient anion, under two autodetachments, ultimately triggers the formation of positively charged fragments. The reaction e (-) + AB -> AB(-)* -> AB* + e(-) -> A(+) B + 2e(-) is supported by both experimental data and scattering calculations.

EUROPEAN PHYSICAL JOURNAL D 76[2], 19, 2022. DOI: 10.1140/epjd/s10053-022-00353-2

[P063-2022] "On the mechanical properties and fracture patterns of the nonbenzenoid carbon allotrope (biphenylene network): a reactive molecular dynamics study"

Pereira Junior, M. L.; Cunha, W. F. da; Sousa, R. T. de; Nze, G. D. A.; **Galvao, D. S.***; Ribeiro, Junior, L. A.

Recently, a new two-dimensional carbon allotrope named biphenylene network (BPN) was experimentally realized. The BPN structure consists of four-, six-, and eight-membered rings of sp(2)-hybridized carbon atoms. In this work, we carried out fully-atomistic reactive (ReaxFF) molecular dynamics simulations to study the mechanical properties and fracture patterns of non-defective and defective (nanocracks) BPN. Results show that, under uniaxial tensile loading, BPN is converted into four distinct morphologies before fracture starts. This conversion process is dependent on the stretching direction. Some of the formed structures contain mainly eight-membered rings, which have different shapes in each morphology. In one of them, a graphitization process occurs before the complete fracture. Importantly, in the presence of nanocracks, no new morphologies are formed. BPN exhibits a distinct fracture process when contrasted to graphene. After the critical strain threshold, the graphene transitions from an elastic to a brittle regime, while BPN can exhibit different inelastic stages. These stages are associated with the appearance of new morphologies. However, BPN shares some of the exceptional graphene properties. BPN Young's modulus and melting point are comparable to graphene, about 1019.4 GPa and 4024 K, respectively.

NANOSCALE 14[8], 3200-3211, 2022. DOI: 10.1039/d1nr07959j

[P064-2022] "Perturbative structure of two- and four-point functions of color charge in a non-Gaussian small-x action"

Giannini, A. V.*; Nara, Y.

We compute the perturbative expansion of the two- and four--point functions of color charges in the Color Glass Condensate framework considering the quartic correction to the McLerran-Venugopalan (MV) model of Gaussian color charge fluctuations. Expressions for these correlators in the perturbative expansion for small and large non-Gaussian color charge fluctuations are derived for arbitrary orders in perturbation theory. We explicitly show that the perturbative series does not converge at higher orders as expected. We apply the Borel-Pade resummation method to our problem to construct a convergent series. It is shown that the fully non-perturbative solution can be described by the Borel--Pade approximants constructed from the first few terms of the perturbative series for small non-Gaussian fluctuations.

EUROPEAN PHYSICAL JOURNAL C 82[2], 109, 2022. DOI: 10.1140/epjc/s10052-022-10017-5

[P065-2022] "Prompt D-0, D+, and D*(+) production in Pb--Pb collisions at root S-NN=5.02 TeV"

Acharya, S.; Adamova, D.; **Chinellato, D. D.*; Guardiano, G. G.*; Jahnke, C.*; Takahashi, J.*;** et al. ALICE Collaboration

The production of prompt D-0, D+, and D*(+) mesons was measured at midrapidity (vertical bar y vertical bar < 0.5) in Pb-Pb collisions at the centre-of-mass energy per nucleon-nucleon pair root S-NN = 5.02 TeV with the ALICE detector at the LHC. The D mesons were reconstructed via their hadronic decay channels and their production yields were measured in central (0-10%) and semicentral (30-50%) collisions. The measurement was performed up to a transverse momentum (p(T)) of 36 or 50 GeV/c depending on the D meson species and the centrality interval.

For the first time in Pb-Pb collisions at the LHC, the yield of D-0 mesons was measured down to p(T) = 0, which allowed a model-independent determination of the p(T)-integrated yield per unit of rapidity (dN/dy). A maximum suppression by a factor 5 and 2.5 was observed with the nuclear modification factor (R-AA) of prompt D mesons at p(T) = 6-8 GeV/c for the 0-10% and 30-50% centrality classes, respectively. The D-meson R-AA is compared with that of charged pions, charged hadrons, and J/psi mesons as well as with theoretical predictions. The analysis of the agreement between the measured R-AA, elliptic (v(2)) and triangular (v(3)) flow, and the model predictions allowed us to constrain the charm spatial diffusion coefficient D-s. Furthermore the comparison of R-AA and v(2) with different implementations of the same models provides an important insight into the role of radiative energy loss as well as charm quark recombination in the hadronisation mechanisms.

JOURNAL OF HIGH ENERGY PHYSICS [1], 174, 2022. DOI: 10.1007/JHEP01(2022)174

[P066-2022] "Quantum-chemistry study of the ground and excited state absorption of distyrylbenzene: Multi vs single reference methods"

Roldao, J. C.; **Oliveira, E. F.***; Milian-Medina, B.; Gierschner, J.; Roca-Sanjuan, D.

State-of-the-art complete active space self-consistent field/complete active space second order perturbation theory (CASPT2) calculations are used to investigate the role of double excitations on the ground state absorption (GSA) and excited state absorption (ESA) spectra of distyrylbenzene, an important prototype medium-sized pi-conjugated organic compound for optoelectronics. The multi-reference results are compared with linear and quadratic response time-dependent density functional theory (DFT) results, revealing an incomplete description of the electronic transitions in the latter. Careful selection of the active space and basis set in the CASPT2 approach allows for a reliable description of the GSA and ESA features; cost-effective DFT-based geometries can be utilized without a significant loss of accuracy. Double excitations are shown to play a pivotal role already for higher excited states in the GSA spectrum, however, without a relevant impact on the discernible spectral features. In the ESA, which shows a much more complex electronic situation, the crucial importance of double (and higher) excitations in all relevant electronic transitions, indeed, mandates a multiconfigurational treatment as done in the present benchmark study.

JOURNAL OF CHEMICAL PHYSICS 156[4], 044102, 2022. DOI: 10.1063/5.0073189

[P067-2022] "Sample Concentration Affects Optical Gain Results in Colloidal Nanomaterials: Circumventing the Distortions by Below Band Gap Excitation"

Nagamine, G.*; Ferreira, T. A. C.*; Almeida, D. B.*; Lemus, J. C.*; Chang, J. H.; Jeong, B.; Bae, W. K.; **Padilha, L. A.***

Ultrafast spectroscopy studies have been key to the development of optical materials, including colloidal semiconductor nanocrystals (NCs) engineered for lighting and light-harvesting technologies. Several physical processes, which are revealed by ultrafast spectroscopy in NCs, are highly dependent on the average number of excitons created per NC, including optical gain properties and multiexciton interactions. Consequently, proper considerations regarding NC populations are necessary to avoid misinterpretations. In this paper, we present an experimental and theoretical analysis of the influence of the sample optical density (OD) at the excitation energy on the results of ultrafast spectroscopy studies in NCs. We show that the pump beam depletion caused by high ODs can drastically change the results from transient absorption (TA) experiments leading to data misinterpretations, such as the overestimation of the optical gain threshold. Based on that, we propose a robust modification on the TA technique, which allows for an OD-independent characterization, free of distortions. The modification consists of pumping the sample below its band gap energy, limiting the electronic excitation to a two-photon absorption process, resulting in an effectively zero OD for the pump beam and a uniform excitation in the direction of the beam propagation. Consequently, an undistorted TA signal is produced, allowing for precise characterization of NCs, including the gain/absorption cross section, gain coefficient, and gain threshold. Furthermore, the uniform excitation allows for higher signal-to-noise ratio, independent of the sample concentration.

ACS PHOTONICS 9[1], 156-162, 2022. DOI: 10.1021/acsphotonics.1c01293

[P068-2022] "Search for flavor-changing neutral current interactions of the top quark and the Higgs boson decaying to a bottom quark-antiquark pair at root s=13 TeV"

Tumasyan, A.; Adam, W.; **Chinellato, J. A.***; et al. CMS Collaboration

A search for flavor-changing neutral current interactions of the top quark (t) and the Higgs boson (H) is presented. The search is based on a data sample corresponding to an integrated luminosity of 137 fb(-1) recorded by the CMS experiment at the LHC in proton-proton collisions at root s = 13TeV. Events containing exactly one lepton (muon or electron) and at least three jets, among which at least two are identified as originating from the hadronization of a bottom quark, are analyzed. A set of deep neural networks is used for kinematic event reconstruction, while boosted decision trees distinguish the signal from the background events. No significant excess over the background predictions is observed, and upper limits on the signal production cross sections are extracted. These limits are interpreted in terms of top quark decay branching fractions (B) to the Higgs boson and an up (u) or a charm quark (c). Assuming one nonvanishing extra coupling at a time, the observed (expected) upper limits at 95% confidence level are B(t -> Hu) < 0.079 (0.11)% and B(t -> Hc) < 0.094 (0.086)%.

JOURNAL OF HIGH ENERGY PHYSICS [2], 169, 2022. DOI: 10.1007/JHEP02(2022)169

[P069-2022] "Search for long-lived particles decaying to leptons with large impact parameter in proton-proton collisions at root s=13 TeV"

Tumasyan, A.; Adam, W.; **Chinellato, J. A.***; et al. CMS Collaboration

A search for new long-lived particles decaying to leptons using proton-proton collision data produced by the CERN LHC at root s = 13 TeV is presented. Events are selected with two leptons (an electron and a muon, two electrons, or two muons) that both have transverse impact parameter values between 0.01 and 10 cm and are not required to form a common vertex. Data used for the analysis were collected with the CMS detector in 2016, 2017, and 2018, and correspond to an integrated luminosity of 118 (113) fb(-1) in the ee channel (e mu and mu mu channels). The search is designed to be sensitive to a wide range of models with displaced e mu ee, and mu mu final states. The results constrain several well-motivated models involving new long-lived particles that decay to displaced leptons. For some areas of the available phase space, these are the most stringent constraints to date.

EUROPEAN PHYSICAL JOURNAL C 82[2], 153, 2022. DOI: 10.1140/epjc/s10052-022-10027-3

[P070-2022] "Search for strongly interacting massive particles generating trackless jets in proton-proton collisions at root s=13 TeV"

Tumasyan, A.; Adam, W.; **Chinellato, J. A.***; et al. CMS Collaboration

A search for dark matter in the form of strongly interacting massive particles (SIMPs) using the CMS detector at the LHC is presented. The SIMPs would be produced in pairs that manifest themselves as pairs of jets without tracks. The energy fraction of jets carried by charged particles is used as a key discriminator to suppress efficiently the large multijet background, and the remaining background is estimated directly from data. The search is performed using proton-proton collision data corresponding to an integrated luminosity of 16.1 fb(-1), collected with the CMS detector in 2016. No significant excess of events is observed above the expected background. For the simplified dark matter model under consideration, SIMPs with masses up to 100 GeV are excluded and further sensitivity is explored towards higher masses.

EUROPEAN PHYSICAL JOURNAL C 82[3], 213, 2022. DOI: 10.1140/epjc/s10052-022-10095-5

[P071-2022] "Stability of oxygenated groups on pristine and defective diamond surfaces"

Oliveira, E.*; Li, C. X.; Zhang, X.; Puthirath, A.; Neupane, M. R.; Weil, J.; Birdwell, A. G.; Ivanov, T.; Kong, S.; Grey, T.; Kannan, H.; Vajtai, R.; **Galvao, D. S.***; Ajayan, P.

The surface functionalization of diamonds has been extensively studied through a variety of techniques, such as controlled oxidation. Several oxygen groups have been detected on oxidized diamonds, such as C-O-C (ester), C=O (ketonic), and C-OH (hydroxyl). However, the composition and relative concentration of these groups on diamond surfaces can be affected by the type of oxygenation treatment and the diamond surface quality. To investigate the stability of the oxygenated groups at specific diamond surfaces, we evaluated through fully atomistic reactive (ReaxFF force field) molecular mechanics (FARMM) simulations, the formation energies of the C=O, C-O-C, and C-OH groups on pristine and defective diamond surfaces (110), (111), and (311). According to our findings, the C-OH group has the lowest formation energy on a perfect (110) surface, while the C-O-C is favored on a defective surface. As for the (111) surface, the C-O-C group is the most stable for both pristine and defective surfaces. Similarly, C-O-C group is also the most stable one on the defective/perfect (311) surface. In this way, our results suggest that if, in a diamond film, the (110) surface is the major exposed facet, the most adsorbed oxygen group could be either C-OH or C-O-C, in which the C-O-C would depend on the level of surface defects.

MRS ADVANCES, 2022. Acesso antecipado. DOI: 10.1557/s43580-022-00242-1

[P072-2022] "Study of quark and gluon jet substructure in Z plus jet and dijet events from pp collisions"

Tumasyan, A.; Adam, W.; **Chinellato, J. A.***; et al. CMS Collaboration

Measurements of jet substructure describing the composition of quark- and gluon-initiated jets are presented. Proton-proton (pp) collision data at root s = 13 TeV collected with the CMS detector are used, corresponding to an integrated luminosity of 35.9 fb(-1). Generalized angularities are measured that characterize the jet substructure and distinguish quark- and gluon-initiated jets. These observables are sensitive to the distributions of transverse momenta and angular distances within a jet. The analysis is performed using a data sample of dijet events enriched in gluon-initiated jets, and, for the first time, a Z+jet event sample enriched in quark-initiated jets. The observables are measured in bins of jet transverse momentum, and as a function of the jet radius parameter. Each measurement is repeated applying a "soft drop" grooming procedure that removes soft and large angle radiation from the jet. Using these measurements, the ability of various models to describe jet substructure is assessed, showing a clear need for improvements in Monte Carlo generators.

JOURNAL OF HIGH ENERGY PHYSICS [1], 188, 2022. DOI: 10.1007/JHEP01(2022)188

[P073-2022] "Testing effects of Lorentz invariance violation in the propagation of astroparticles with the Pierre Auger Observatory"

Abreu, P.; Aglietta, M.; **Bonneau, A., L.*; Chinellato, J. A.*; Franco, D. de O.*; Dobrigkeit, C.*; Fauth, A. C.*; Payeras, A. M.*; Muller, M. A.***; et al. Pierre Auger Collaboration; Pierre Auger Collaboration

Lorentz invariance violation (LIV) is often described by dispersion relations of the form E-i(2) = m(i)(2) + p(i)(2) + delta E-i,n(2+ n) with delta different based on particle type i, with energy E, momentum p and rest mass m. Kinematics and energy thresholds of interactions are modified once the LIV terms become comparable to the squared masses of the particles involved. Thus, the strongest constraints on the LIV coefficients delta(i,n) tend to come from the highest energies. At sufficiently high energies, photons produced by cosmic ray interactions as they propagate through the Universe could be subluminal and unattenuated over cosmological distances. Cosmic ray interactions can also be modified and lead to detectable fingerprints in the energy spectrum and mass composition observed on Earth. The data collected at the Pierre Auger Observatory are therefore possibly sensitive to both the electromagnetic and hadronic sectors of LIV. In this article, we explore these two sectors by comparing the energy spectrum and the composition of cosmic rays and the upper limits on the photon flux from the Pierre Auger Observatory with simulations including LIV. Constraints on LIV parameters depend strongly on the mass composition of cosmic rays at the highest energies. For the electromagnetic sector, while no constraints can be obtained in the absence of protons beyond 10(19) eV, we obtain delta(gamma,0) > -10-21, delta(gamma,1) > -10(-4)0 eV(-1) and delta(gamma,2) > -10(-58) eV(-2) in the case of a subdominant proton component up to 10(20) eV. For the hadronic sector, we study the best description of the data as a function of LIV coefficients and we derive constraints in the hadronic sector such as delta(had,0) < 10(-1)9, delta(had),1 < 10-38 eV(-1) and delta(had),2 < 10-57 eV(-2) at 5 sigma CL.

JOURNAL OF COSMOLOGY AND ASTROPARTICLE PHYSICS [1], 023, 2022. DOI: 10.1088/1475-7516/2022/01/023

[P074-2022] "The case of SU(3) criticality in spin-2 chains"

Li, C. S.; Quito, V. L.; **Miranda, E.*;** Pereira, R.; Affleck, I.; Lopes, P. L. S.

It was proposed by Chen et al., [Phys. Rev. Lett. 114, 145301 (2015)] that spin-2 chains display an extended critical phase with enhanced SU(3) symmetry. This hypothesis is highly unexpected for a spin-2 system and, as we argue, would imply an unconventional mechanism for symmetry emergence. Yet, the absence of convenient critical points for renormalization group perturbative expansions, allied with the usual difficulty in the convergence of numerical methods in critical or small-gapped phases, renders the verification of this hypothetical SU(3)-symmetric phase a non-trivial matter.

By tracing parallels with the well-understood phase diagram of spin-1 chains and searching for signatures robust against finite--size effects, we draw criticism on the existence of this phase. We perform non-Abelian density matrix renormalization group studies of the multipolar static correlation function, energy spectrum scaling, single-mode approximation, and entanglement spectrum to shed light on the problem. We determine that the hypothetical SU(3) spin-2 phase is, in fact, dominated by ferro-octupolar correlations and also observe a lack of Luttinger-liquid-like behavior in correlation functions that suggests that is perhaps not critical. We further construct an infinite family of spin -S systems with similar ferro-octupolar-dominated quasi-SU(3)-like phenomenology; curiously, we note that the spin-3 version of the problem is located in a subspace of exact G(2) symmetry, making this a point of interest for search of Fibonacci topological properties in magnetic systems.

PHYSICAL REVIEW B 105[8], 085140, 2022. DOI: 10.1103/PhysRevB.105.085140

[P075-2022] "Tunable Anomalous Scattering and Negative Asymmetry Parameter in a Gain-Functionalized Low Refractive Index Sphere"

Ali, R.*

Usually, low refractive index passive spheres exhibit strong forward scattering and a positive asymmetry parameter due to weak interference between the electric and magnetic scattering channels. In this work, we investigate, analytically and numerically, the forward scattering of light by a gain--functionalized low refractive index dielectric sphere. It is shown that by tuning the optical gain one can optimize the interference, which provides a novel paradigm to achieve the zero forward scattering and negative asymmetry parameter even for a low refractive index sphere. As a result, a low-density collection of such identical back scatterers provides an anomalous regime, where the scattering mean free path and extinction mean free path are greater than the transport mean free path. Furthermore, we also provide the numerical guideline to achieve the larger extinction mean free path without achieving preferential back-scattering.

ACS OMEGA 7[2], 2170-2176, 2022. DOI: 10.1021/acsomega.1c05662

[P076-2022] "Understanding and visualizing the statistical analysis of SN1987A neutrino data"

Santos, M. V. dos*; Holanda, P. C. de*

The SN1987A detection through neutrinos was an event of great importance in neutrino physics, being the first detection of neutrinos created outside our solar system, and then inaugurating the era of experimental neutrino astronomy. The data have been largely studied in many different analysis, and has presented several challenges in different aspects, since both supernova explosion dynamics and neutrino flavour conversion in such extreme environment still have many unknowns. In addition, the low statistics also invoke the need of unbinned statistical methods to compare any model proposal with data. In this paper we focus on a discussion about the most used statistical analysis interpretation, presenting a pedagogical way to understand and visualize this comparison.

EUROPEAN PHYSICAL JOURNAL C 82[2], 145, 2022. DOI: 10.1140/epjc/s10052-022-10091-9

Correções

[Co001-2022] "In Vivo and In Vitro Taste Assessment of Artesunate-Mefloquine, Praziquantel, and Benznidazole Drugs for Neglected Tropical Diseases and Pediatric Patients (vol 23, 22, 2022)"

Boniatti, J.; Tappin, M. R. R.; Teixeira, R. G. D. da S.; Gandos, T. D. A.; Rios, L. P. S.; Ferreira, I. A. M.; Oliveira, K. C.; Calil--Elias, S.; Santana, A. K. M.; Fonseca, L. B. da; **Shimizu, F. M.***; Carr, O.; Oliveira Jr., O. N.; Dantas, F. M. L.; Amendoeira, F. C.; Vicosa, A. L.

AAPS PHARMSCITECH 23[1], 64, 2022. DOI: 10.1208/s12249-022-02216-w

[Co002-2022] "The molecular structure of the surface of water-ethanol mixtures (vol 23, pg 11568, 2021)"

Kirschner, J.; **Gomes, A. H. A.***; Marinho, R. R. T.; Bjorneholm, O.; Agren, H.; Carravetta, V.; Ottosson, N.; **Brito, A. N. de***; Bakker, H. J.

PHYSICAL CHEMISTRY CHEMICAL PHYSICS 24[11], 7164-7164, 2022. DOI: 10.1039/d2cp90046g

***Autores da comunidade IFGW**
Fonte: Web of Science on-line (WOS)

Defesas de Dissertações do IFGW

[D003-2022] "Estudo da separação de múons e elétrons em tanque de radiação Cherenkov na água"
Aluno: Fernando Lock Miletto
Orientador: Prof. Dr. Anderson Campos Fauth
Data: 11/03/2022

[D004-2022] "Cintilação de Argônio Líquido com dopagem de xenônio: Análise de forma de onda e emissão de luz utilizando o coletor de photons X-ARAPUCA"
Aluno: Greg de Souza
Orientador: Prof. Dr. Ettore Segreto
Data: 17/03/2022

[D005-2022] "Condições iniciais utilizando PYTHIA para simulações hidrodinâmicas"
Aluno: Luiza Lober de Souza Piva
Orientador: Prof. Dr. David Dobrigkeit Chinellato
Data: 18/04/2022

Defesas de Teses do IFGW

[T004-2022] "Dosimetry in contemporary X-ray breast imaging modalities by monte carlo simulation"
Aluno: Rodrigo Trevisan Massera
Orientador: Profa. Dra. Alessandra Tomal
Data: 10/03/2022

[T005-2022] "Investigação da neuroplasticidade funcional no cérebro humano com espectroscopia no infravermelho próximo"
Aluno: Sérgio Luis Novi Junior
Orientador: Prof. Dr. Rickson Mesquita
Data: 17/03/2022

[T006-2022] "Crescimento e caracterização de monocamada de HfS2 sobre Ag (111)"
Aluno: Isabela da Costa Tonon
Orientador: Prof. Dr. Abner de Siervo
Data: 18/03/2022

[T007-2022] "Simulações Atomísticas de Gelo Hexagonal e Matrizes de Cimento Alternativos"
Aluno: Jéssica Santos Rego
Orientador: Prof. Dr. Maurice de Koning
Data: 25/03/2022

[T008-2022] "Propriedades magnéticas de sistemas complexos com topologia não trivial"
Aluno: Jean Carlo Souza
Orientador: Prof. Dr. Pascoal José Giglio Pagliuso
Data: 12/04/2022

Fonte: Portal IFGW/Pós-graduação - Agenda de Colóquios, Defesas e Seminários.
Disponível em: http://portal.ifi.unicamp.br/pos-graduacao

Cadastre-se como leitor, e receba os avisos da publicação de novos números por e-mail.

Abstracta

Instituto de Física
Diretor: Profa. Dra. Mônica Alonso Cotta
Diretora Associada: Prof. Dr. Marcos Cesar de Oliveira
Universidade Estadual de Campinas - UNICAMP
Cidade Universitária Zeferino Vaz
13083-859 - Campinas - SP - Brasil
e-mail: secdir@ifi.unicamp.br
Fone: +55 19 3521-5300

Publicação

Biblioteca do Instituto de Física Gleb Wataghin
http://portal.ifi.unicamp.br/biblioteca
Instagram: @bif.unicamp
Telegram: t.m/bifunicamp

Diretora Técnica: Sandra Maria Carlos Cartaxo
Coordenadora da Comissão de Biblioteca: Profa. Dra. Arlene Cristina Aguilar

Elaboração:
Maria Graciele Trevisan (Bibliotecária)
contato: infobif@ifi.unicamp.br